ELSEVIER

Nuclear Instruments and Methods in Physics Research A 487 (2002) 450–456

NUCLEAR INSTRUMENTS & METHODS IN PHYSICS RESEARCH Section A

www.elsevier.com/locate/nima

Characterization of superconducting tunnel junction X-ray detectors by means of monochromatized undulator radiation

M. Veldkamp[a,1], B. Beckhoff[a,*], R. Fliegauf[a], G. Ulm[a], M. Frank[b], S. Friedrich[b], S.E. Labov[b]

[a] *Physikalisch-Technische Bundesanstalt, Abbestraße 2-12, 10587 Berlin, Germany*
[b] *Lawrence Livermore National Laboratory, P.O. Box 808, L-418, Livermore, CA 94551, USA*

Received 12 October 2001; received in revised form 19 November 2001; accepted 10 December 2001

Abstract

A superconducting tunnel junction X-ray detector system was designed to match current energy resolution, count rate and UHV requirements in soft X-ray spectroscopy. It employs a two-stage adiabatic demagnetization refrigerator with a 23 cm long cold finger to operate the detector inside a sample chamber for X-ray fluorescence measurements. This cryogenic detector system was characterized in the energy range from 100 eV to 900 eV with respect to its energy resolution ranging from 12 eV to 25 eV FWHM, count rate capability up to 80 kcps and absolute detection efficiency using undulator radiation monochromatized by means of a plane grating monochromator beamline. Collimating the beam to the detector area improves the energy resolution by about 10%. The potential of this novel detector for beamline characterization was investigated.

PACS: 85.25.Oj; 07.85.Qe; 78.70.En

Keywords: Superconducting tunnel junction (STJ); Detector calibration; X-ray fluorescence analysis (XRF); Beamline characterization; Synchrotron radiation

1. Introduction

In 1999, the Physikalisch-Technische Bundesanstalt (PTB), Germany's national metrology institute, began operating a plane grating monochromator (PGM) beamline [1,2] for undulator radiation at BESSY II offering high spectral purity radiation in the photon energy range from 30 eV to 1900 eV.

The first spectroscopic objective was to determine the detection sensitivities of X-ray fluorescence (XRF) trace element analysis for light elements. The detection limits of total reflection XRF for single-element analysis of light elements between C and Al were found to be in the low picogram or even sub-picogram range [3]. However, in the corresponding energy range between 270 eV and about 1500 eV, the energy resolution of conventional semiconductor detectors, such as Si(Li) and HPGe detectors, is not sufficient to

*Corresponding author. Fax: +49-30-639-250-82.
E-mail address: burkhard.beckhoff@ptb.de (B. Beckhoff).
[1] Present address: Infineon Technologies SC300 GmbH & Co KG, Königsbrücker Str. 180, 01099 Dresden, Germany

0168-9002/02/$ - see front matter
PII: S0168-9002(01)02197-0

discriminate simultaneously K-shell fluorescence lines of light elements from L-shell fluorescence lines of transition metals, as is typical in multi-element specimens.

Cryogenic superconducting tunnel junction (STJ) detectors may contribute to overcoming this restriction in low-energy XRF due to their high-energy resolution. The PTB began operating such a cryogenic STJ detector system, based on a two-stage adiabatic demagnetization refrigerator (ADR), designed and provided by Lawrence Livermore National Laboratory [4] in late 1999. The STJ is operated at temperatures between 80 mK and 400 mK at the end of a cold finger inside a liquid He and a liquid N_2-cooled shield with a total length of 23 cm and a diameter of 33 mm, allowing for effective XRF detection in a UHV environment.

Superconducting transition edge sensors (TES) are an alternative low-temperature detector technology [5]. Compared to TES detectors, which show a slightly better energy resolution, STJ detectors intrinsically have higher count rate capabilities. Whereas the present limit for TES X-ray detectors is of the order of 1000 cps, STJs can be operated at rates that are more than an order of magnitude higher with only a moderate degradation of the energy resolution [6]. A present drawback of STJs is the appearance of artifacts in the pulse height spectra originating from photons absorbed in the substrate or in the Nb contact leads. Additionally, the probability of line splitting and broadening increases with increasing energy of the incident photon because the absorption capability of the top Nb-layer and that of the Al layers usually decreases and the photon may reach the bottom Nb-layer. As the response of the bottom Nb-layer may be slightly different from that at the top Nb-layer, line splitting occurs when both responses superimpose. In future devices such artifacts could be significantly reduced by using STJs that have a top layer with increased X-ray stopping power, such as thicker niobium or tantalum [7]. Another possibility would be to add a thick lead absorber layer on top of an aluminum STJ, as has been demonstrated recently by the TU Munich group [8]. While this latter approach is expected to avoid most of the artifact problems, it comes at the cost of some reduction in speed. In spite of the small artifact problems with present generation STJ detectors, their high count-rate capability combined with an energy resolution of about 10 eV FWHM makes STJs the detectors of choice for experiments based on synchrotron radiation. Here, we report the first set of characterization experiments with our new STJ detector system using undulator radiation monochromatized by the PGM beamline.

2. Superconducting tunnel junctions

We will only give a brief outline of the basic detection principles of STJ detectors here. A more detailed description can be found in Ref. [6]. The STJ-detector layout is shown in Fig. 1. The

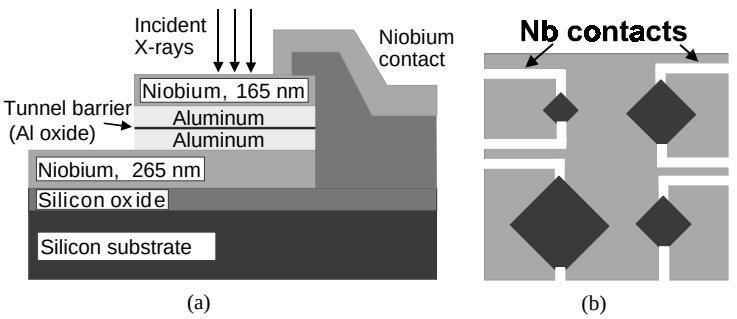

Fig. 1. Schematics of an STJ detector: (a) shows a cross-section of an Nb/Al/Al_2O_3/Al/Nb tunnel junction. Four such junctions with areas ranging from 70×70 to $200 \times 200\,\mu m^2$ are located on one detector chip. The Al-layer thicknesses are 50 nm ; (b) is a top view also showing the wiring of the junctions.

detector is operated at temperatures of about 100 mK, where all metallic layers within the detector are superconducting. Incident X-ray photons are absorbed in the top Nb layer and, following complex energy down-conversion processes, transfer their energy into the creation of excess quasiparticles. The number of quasiparticles generated is proportional to the photon energy, allowing for energy-resolved measurements. Due to the smaller energy gap of Al as compared to Nb, the quasiparticles are trapped within the Al layer, leading to a concentration of the excess quasiparticles close to the tunnel barrier. Whenever these quasiparticles quantum-mechanically tunnel through the oxide barrier, the current temporarily increases. This excess current is detected by a current-sensitive preamplifier with the signal height proportional to the energy of the incident photon.

Compared to conventional semiconductor detectors, the most prominent feature of STJ detectors is their improved energy resolution. The average energy required to produce an electron–hole pair in an Si(Li) detector is 3.8 eV, i.e. a 1 keV photon will produce about 260 charge carriers. The energy required to produce an excess quasiparticle in Nb is only about 2.71 meV, being 1.75 times the superconducting energy gap of Nb [9]. Hence, a 1 keV photon produces about 3.7×10^5 charge carriers. Due to better statistics, the energy resolution can be improved by more than an order of magnitude. Measured energy resolutions of 5 eV FWHM at 300 eV photon energy for Ta-based STJs [10], of 6 eV FWHM at a photon energy of 277 eV for Nb-based STJs [6] and of 12 eV FWHM at an energy of 5.9 keV [8,11] for Al-based STJs have been reported. The perspectives of STJ detectors with particular emphasis on the absorber materials have been discussed in Ref. [12].

3. Experimental arrangement and initial results

We have examined an Nb-based STJ as shown in Fig. 1 with an area of $141 \times 141\ \mu m^2$. The STJ is operated in a two-stage ADR cryostat with the detector positioned at the end of a 23 cm long Cu cold finger that also carries the detector magnet needed to suppress the DC Josephson current for stable STJ operation. The detector assembly is surrounded by both a liquid He and a liquid N_2-cooled Cu radiation shield. With this design, it is possible to operate the STJ detector in XRF geometries allowing for small distances between sample and detector, i.e. for relatively high solid angle acceptances of the detector. Furthermore, the distance between sample and detector can be easily changed while maintaining UHV conditions. We placed a total of three infrared radiation (IR) blocking windows, one at each shield and one on the 0.1 K cold stage, in front of the STJ-detector to reduce the heat load and the excess noise caused by the absorption of IR photons from the UHV chamber at room temperature. Each window is composed of 200 nm parylene-N coated with 20 nm Al. The windows need to have a certain thickness to effectively shield the detector against IR radiation, yet they should be as thin as possible to ensure a high transmittance for soft X-rays. In the near future, we shall investigate the possibility to increase the solid angle of acceptance efficiently by combining polycapillary optics with such a novel kind of cryogenic detector [5].

The choice of bias voltage and the field of the detector magnet are important for the performance of the detector. Fig. 2 shows the measured

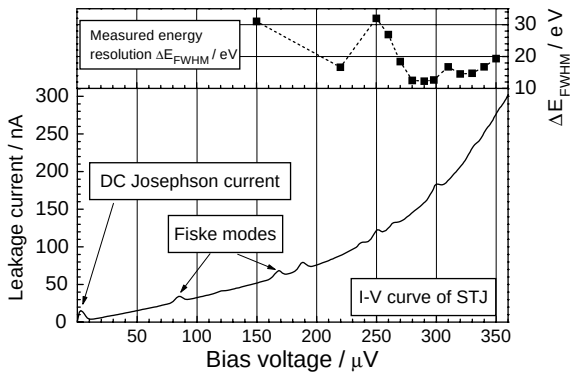

Fig. 2. Measured I–V curve of an STJ detector with an effective area of $141 \times 141\ \mu m^2$ examined at a magnetic field of 14 mT. The top inset shows the measured energy resolution (square data points) as a function of bias voltage determined at a photon energy of 130 eV. (The dashed line is just a guide for the eye.)

dependence of the DC leakage current of the STJ on the DC bias voltage for an optimized magnetic field of 14 mT. The I–V curve of this STJ shows the typical features already reported in the literature. Close to a bias voltage of 0 V, we observe a small remaining DC Josephson current originating from tunneling Cooper pairs. In addition, the so-called Fiske mode resonances can be found at 85 μV, 170 μV, 190 μV, etc. It has already been demonstrated that the STJ performance is significantly reduced whenever the bias voltage is set close to Fiske modes [13]. The inset at the top of Fig. 2 shows the detector resolution as a function of bias voltage. It indicates that one factor that reduces detector performance is biasing the STJ at a Fiske mode voltage, as has been observed before [13].

For our measurements, we have chosen a bias voltage of 290 μV. At this voltage setting, the energy resolution is high and does not change significantly for small drifts of the bias voltage of order $\pm 1.5\,\mu V$ (rms) during operation. With this setup, we have examined the energy resolution ΔE of our Nb-based STJ detector as a function of the photon energy (cf. Fig. 3). An estimate for the electronic noise was determined by injecting well-defined charge pulses from an electronic pulser into the STJ preamplifier input during the X-ray measurements and measuring the line width of the resulting "pulser line" in the X-ray spectrum. (Note that this is a commonly used convenient way to measure the "electronic noise". More precisely, it measures the baseline noise and also includes baseline fluctuations caused by pulse pile-up at high count rates.) The intrinsic resolution was obtained by subtracting the measured electronic noise contribution (i.e., the pulser line width) from the measured total resolution (i.e., X-ray line width). Using a CCD we had measured a beam size on the site of the detector of about $0.5 \times 0.5\,mm^2$, which is approximately ten times larger than the detector area. Without collimation of the incident beam, an energy resolution well below 20 eV can be obtained for photon energies up to 700 eV. Presently, the ΔE value obtained is about 5 times higher than the fundamental limit set by fluctuations in the charge generation of tunneling processes. The present energy resolution is poorer compared to the results obtained with

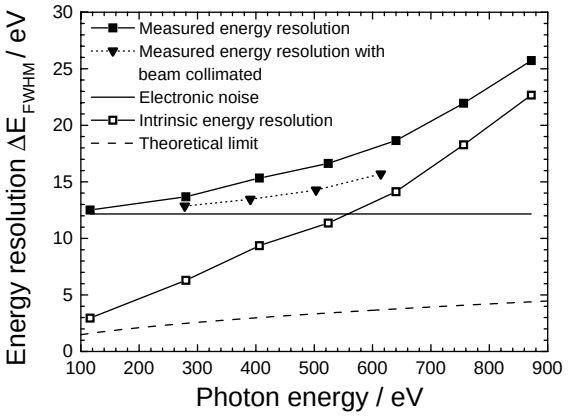

Fig. 3. Energy resolution of the STJ detector measured as a function of photon energy. Two experiments are shown. The first experiment was performed at a beam size of about $0.5 \times 0.5\,mm^2$, i.e. not only the detector area but also large parts of the surrounding Si substrate have been illuminated by the beam. The measured energy resolution in this case (solid squares) increases strongly with photon energy. The measured electronic noise (solid line) and calculated intrinsic energy resolution (open squares) refer to this experiment. The second experiment was conducted using a collimating pinhole in front of the detector reducing the spot of the beam to the detector area. In this case (solid triangles), not only the energy resolution is improved, but also the slope of the measured energy resolution with photon energy decreases.

same size STJ detectors from the same wafer located in the center of a conventional ADR cryostat [6]. The resolution has been improved using thicker IR blocking windows and reducing the solid angle of acceptance of the detector for IR radiation. The search for an optimal IR blocking configuration is to be continued in our laboratories. We have also collimated the incident beam to about the size of the detector area. Here, the measured energy resolution was improved by about 10% in initial experiments. This suggests that some of the increase of ΔE at higher energies may be caused by substrate events, i.e. by photons absorbed in the Si substrate near the STJ detector.

We have obtained promising results for the performance of STJs at high count rates at an incident photon energy of 280 eV (cf. Fig. 4). The count rate quoted here is derived from the total number of events in the spectrum and the active time of the pulse height analyzer. Starting from 14 eV at 200 cps, the energy resolution degraded to

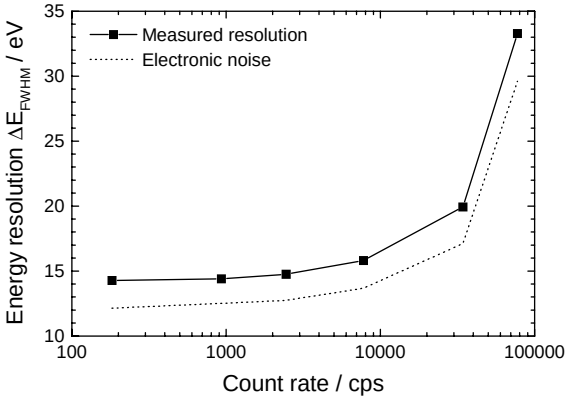

Fig. 4. Energy resolution of the STJ detector as a function of count rate at a fixed energy of 280 eV. The intrinsic detector resolution is determined by subtracting the electronic noise (as measured by the line width of an injected electronic pulser signal) in quadrature from the measured energy resolution.

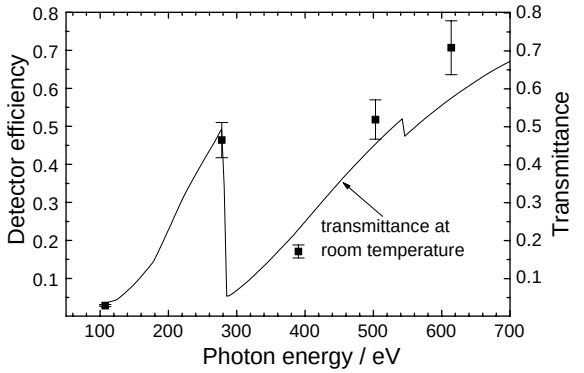

Fig. 5. Absolute detection efficiency of a $141 \times 41\ \mu m^2$ area Nb-based STJ detector including three 200 nm thick parylene N IR blocking windows, each of which is coated with a 20 nm thick Al layer. At the higher energies, bottom Nb-layer events were included in the detector response. For comparison, the experimental transmittance at room temperature of these 3 IR windows is plotted. The transmittance of the film during operation at the temperatures of 77 K, 4 K and 100 mK may be different.

20 eV at 40 kcps. The resolution degraded to about 33 eV at a count rate of 80 kcps due to pile-up. Using pile-up rejection and novel pulse processing electronics, i.e. digital signal processors (DSPs), it may be possible to further improve the high count-rate performance. In addition, DSPs will also provide the possibility of online event discrimination based on rise time differences. This will be a powerful tool for rejecting longer rise time events due to photons absorbed in the substrate and for removing line-splitting artifacts that occur at a higher energy because of photon absorption in the bottom Nb electrode.

To determine the absolute detector efficiency [1], special operation shifts at BESSY II were used, in which the stored electron beam current was severely reduced to adapt the photon flux to the STJ detector count-rate capability. Such a calibration is needed whenever experiments call for the knowledge of the incident, total radiant power, e.g. fluorescence yield measurements or quantitative beamline characterization experiments.

To ensure that the total incident power can be detected by the STJ, we have reduced the beam size to the detector area by placing a pinhole with a diameter of 70 μm in front of the detector. A transfer detector standard behind the pinhole, i.e. a calibrated photodiode, first records the radiant power of monochromatic radiation of high spectral purity at conventional electron beam currents. Subsequently, the electron beam current is reduced assuming that the radiation quality does not change. This assumption implies that the radiant power reduces linearly with the stored electron beam current. Fig. 5 shows the result of the first calibration of the whole STJ detector system. The efficiency was obtained by comparing the incident radiant power detected by the calibrated photodiode behind the pinhole with that detected by the STJ taking the reduced electron beam current into account. The error bars of the data points are dominated by the error of the determined radiant power by using a calibrated photodiode and are assumed to be $\pm 5\%$ of the measured value. The measured efficiency follows roughly the transmittance of the three IR blocking Al-coated parylene N windows, as determined experimentally at room temperature. The deviation of the measured efficiency data may be explained more adequately by assuming a minor thickness reduction due to tension of the windows at low temperatures and additional layers of frozen gas deposited on the coldest windows. This will be the objective of a dedicated investigation in the near future.

4. STJ potential for beamline characterization

Due to their high count-rate dynamics and their high energy resolution, STJ detectors can also be a very valuable tool for beamline characterization. To illustrate this, we measured the spectral purity of the U180 PGM beamline by varying the c_{ff} value of the monochromator at a constant energy. The c_{ff} value is a trigonometric ratio of the incident and diffracted beam angles at the plane grating. It is expected that the spectral purity and flux change with c_{ff} [2]. A representative result for an undulator setting of 5 eV for the first harmonic and the monochromator tuned to 116 eV is shown in Fig. 6. We used a 1200 l/mm Au-coated grating for this experiment. In addition to the first and second diffraction order of the grating, we observe artifacts probably due to photons absorbed in a thin surface layer of the STJ detector [6] having a reduced response.

To determine the spectral purity at the U180-PGM beamline quantitatively, we tuned the monochromator to 130 eV and varied the c_{ff} value between 1.4 and 2.3 as shown in Fig. 7. The measurements suggest that for a maximum suppression of higher orders at simultaneous high flux, a c_{ff} value of 1.4 should be chosen. This results in a suppression of the higher order contributions below 0.5%, well matching the design goals of the PGM beamline. The higher order contribution depicted in Fig. 7 is consistent with similar investigations performed by means of a transmission-grating spectrometer.

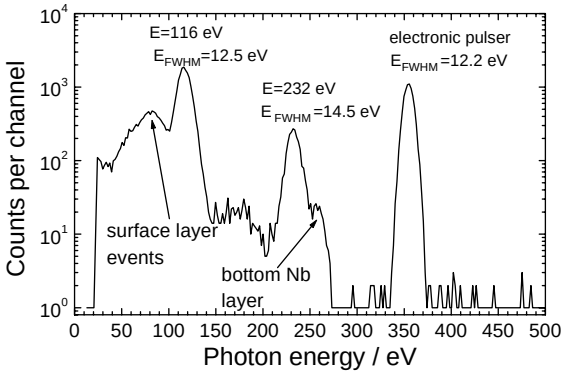

Fig. 6. STJ spectrum showing the detector response at the photon energies of 116 eV (first PGM order) and of 232 eV (second PGM order) registered at c_{ff}-value of 1.5. The respective energy resolutions and some of the artifacts are also depicted.

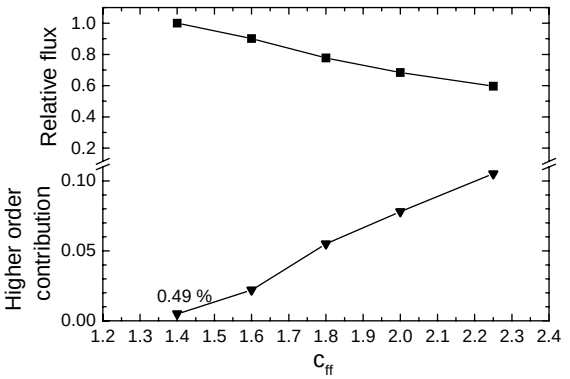

Fig. 7. Measured flux (top graph) and higher order contributions (bottom graph) at the PGM beamline for undulator radiation using an STJ detector system. The first harmonic of the undulator was set to 5 eV and the monochromator was tuned to a fixed energy of 130 eV.

Here, the photon flux recorded by the STJ could not be quoted absolutely because the incident PGM beam profile would have to be smaller than the effective STJ area. In the near future, a more detailed investigation of STJ response functions over a broad energy range of interest shall be performed. Furthermore, STJ detectors calibrated absolutely may contribute effectively to monochromator beamline characterization and XRF applications.

References

[1] B. Beckhoff, R. Klein, M. Krumrey, F. Scholze, R. Thornagel, G. Ulm, Nucl. Instr. and Meth. A 444 (2000) 480.
[2] F. Senf, U. Flechsig, F. Eggenstein, W. Gudat, R. Klein, H. Rabus, G. Ulm, J. Synchrotr Radiat. 5 (1998) 780.
[3] C. Streli, P. Wobrauschek, B. Beckhoff, G. Ulm, L. Fabry, P. Pahlke, X-ray Spectrom. 30 (2001) 24.
[4] S. Friedrich, O. Dury, T. Niedermayr, M.F. Cunningham, M.L. van den Berg, J.N. Ullom, A. Loshak, S.P. Cramer, J.D. Batteux, E. See, M. Frank, S.E. Labov, Nucl. Instr. and Meth. A 467–468 (2001) 1117.
[5] D.A. Wollman, S.W. Nam, D.E. Newbury, G.C. Hilton, K.D. Irwin, N.F. Bergren, S. Deiker, D.A. Rudman, J.M. Martinis, Nucl. Instr. and Meth. A 444 (2000) 145.

[6] M. Frank, L.J. Hiller, J.B. le Grand, C.A. Mears, S.E. Labov, M.A. Lindeman, H. Netel, D. Chow, A.T. Barfknecht, Rev. Sci. Instrum. 69 (1998) 25.
[7] S. Kraft, P. Verhoeve, A. Peacock, N. Rando, D.J. Goldie, R. Hart, D. Glowacka, F. Scholze, G. Ulm, J. Appl. Phys. 86 (1999) 7189.
[8] G. Angloher, P. Hettl, M. Huber, J. Jochum, F.v. Feilitzsch, R.L. Mößbauer, J. Appl. Phys. 89 (2001) 1425.
[9] N. Rando, A. Peacock, A. van Dordrecht, C.L. Foden, R. Engelhardt, B.G. Taylor, P. Gare, J. Lumley, C. Pereira, Nucl. Instr. and Meth. 313 (1992) 173.
[10] P. Verhoeve, et al., IEEE Trans. Appl. Supercond. 9 (1999) 3342.
[11] G. Angloher, B. Beckhoff, M. Bühler, F.v. Feilitzsch, T. Hertrich, P. Hettl, J. Höhne, M. Huber, J. Jochum, R.L. Mößbauer, J. Schnagl, F. Scholze, G. Ulm, Nucl. Instr. and Meth. A 444 (2000) 214.
[12] A. Peacock, Physica B 263–264 (1999) 595.
[13] S. Friedrich, M.F. Cunningham, M. Frank, S.E. Labov, A.T. Barfknecht, S.P. Cramer, Nucl. Instr. and Meth. A 444 (2000) 151.